INTERNATIONAL JOURNAL FOR NUMERICAL METHODS IN FLUIDS, VOL. 20, 157–168 (1995)

APPROXIMATION OF SHALLOW WATER EQUATIONS BY ROE'S RIEMANN SOLVER

D. AMBROSI

CRS4, Via Nazario Sauro 10, 09123 Cagliari, Italy

SUMMARY

The inviscid shallow water equations provide a genuinely hyperbolic system and all the numerical tools that have been developed for a system of conservation laws can be applied to them. However, this system of equations presents some peculiarities that can be exploited when developing a numerical method based on Roe's Riemann solver and enhanced by a slope limiting of MUSCL type. In the present paper a TVD version of the Lax–Wendroff scheme is used and its performance is shown in 1D and 2D computations. Then two specific difficulties that arise in this context are investigated. The former is the capability of this class of schemes to handle geometric source terms that arise to model the bottom variation. The latter analysis pertains to situations in which strict hyperbolicity is lost, i.e. when two eigenvalues collapse into one.

KEY WORDS Shallow water equations Flux difference splitting Open channel flow High resolution schemes

1. INTRODUCTION

In recent years there has been a great effort devoted to the definition of efficient and accurate numerical methods for hyperbolic systems and most of all the Euler equations of gas dynamics. From the mathematical point of view the hyperbolic equations are well known to admit discontinuous solutions and their numerical integration is expected to compute such discontinuities sharply and without oscillations. This result has been achieved by several approaches, which can be grouped into the large family of high-resolution shock-capturing schemes. Therefore it appears natural to apply this knowledge to other hyperbolic systems mathematically modelling different physical phenomena.

When considering shock-capturing schemes, the most popular method for solving hyperbolic systems is probably Roe's solver, originally proposed for approximating the Euler equations.[1] One of its main attractive features is the capability to capture discontinuities without any shock-fitting procedure.

In this paper we want to extend Roe's scheme to the shallow water equations (SWEs), stressing some peculiarities that arise in this context. The straightforward extension of this scheme in the SWE framework has recently been done in two different papers.[2,3] Here we use a limiting procedure slightly different from the one used therein, which allows us to obtain second-order accuracy in time in a single discrete step; this scheme can be seen as a slope limitation of the celebrated Lax–Wendroff scheme.[4] Moreover, we focus on several peculiarities that arise when considering the solution of some typical SWE problems, which have no counterpart in the Euler equations.

CCC 0271–2091/95/020157–12

Received January 1994
Revised August 1994

We consider two different examples in which this situation occurs. The former is the dam break wave on a dry bottom; when drying–wetting is present, two eigenvalues collapse into one and the system of equations is not strictly hyperbolic any more. For this problem we reconsider the classical exact solution using some mathematical tools of hyperbolic systems theory and we compare exact and numerical solutions. The second case we consider is the computation of the still water problem with a sloping bottom. Here the bottom variation is taken into account by a geometric source term. Its effect on the numerical solution of the SWEs by the present approach is described and discussed.

2. SHALLOW WATER EQUATIONS

The SWEs in integral form read

$$\frac{\mathrm{d}}{\mathrm{d}t}\int_{\sigma}\mathbf{u}(\mathbf{x},t)\,d\sigma+\oint_{\Gamma}(\mathbf{f}n_x+\mathbf{g}n_y)\,\mathrm{d}\Gamma=\int_{\sigma}\mathbf{s}(\mathbf{x},t)\,\mathrm{d}\sigma\quad\forall t\in[0,T],\tag{1}$$

where $\Omega\subset\mathbb{R}^2$ is the domain (not necessarily filled by the fluid), σ is any open subset of Ω with boundary Γ and $\mathbf{n}$ is the outward unit normal. Symbol explanation is as follows:

$$\mathbf{u}=(h,\,q_x,\,q_y)^{\mathrm{T}},\tag{2}$$

$$\mathbf{f}=\left(q_x,\,\frac{q_x^2}{h}+\frac{g}{2}h^2,\,\frac{q_xq_y}{h}\right)^{\mathrm{T}},\qquad\mathbf{g}=\left(q_y,\,\frac{q_xq_y}{h},\,\frac{q_y^2}{h}+\frac{g}{2}h^2\right)^{\mathrm{T}},\tag{3}$$

$$\mathbf{s}=\left(0,\,gh\frac{\partial h_0}{\partial x},\,gh\frac{\partial h_0}{\partial y}\right)^{\mathrm{T}}.\tag{4}$$

Here $\mathbf{q}(\mathbf{x},t)$ is the unit-width discharge, $-h_0(x,y)$ is the depth under a reference plane, $\zeta(x,y,t)$ is the elevation over the same reference plane, $h(x,y,t)=h_0+\zeta$ and g is the gravitational acceleration (see Figure 1); the source term accounts for the bottom slope and Γ is the boundary of σ. In the present study we omit to consider the bottom friction and the turbulent dissipation; anyway, from a stability point of view it can be seen that they give a positive contribution to the energy norm.[5]

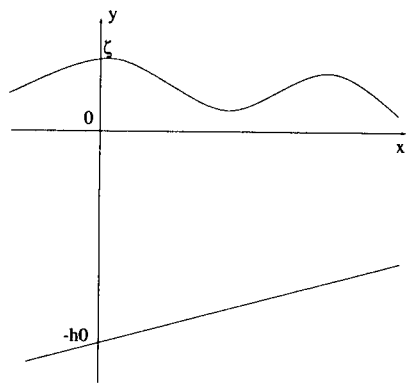

Figure 1. Elevation and depth

We can adimensionalize the SWE system by choosing an appropriate length H. Substituting

$$x' = \frac{x}{H}, \qquad y' = \frac{y}{H}, \qquad t' = \frac{\sqrt{(gH)}}{H} t, \qquad h' = \frac{h}{H}, \qquad \mathbf{q}' = \frac{\mathbf{q}}{H\sqrt{(gH)}}, \tag{5}$$

we get, omitting the prime from now on,

$$\mathbf{f} = \left(q_x, \frac{q_x^2}{h} + \frac{h^2}{2}, \frac{q_x q_y}{h}\right)^{\mathrm{T}}, \qquad \mathbf{g} = \left(q_y, \frac{q_x q_y}{h}, \frac{q_y^2}{h} + \frac{h^2}{2}\right)^{\mathrm{T}}, \tag{6}$$

$$\mathbf{s} = \left(0, h\frac{\partial h_0}{\partial x}, h\frac{\partial h_0}{\partial y}\right)^{\mathrm{T}}. \tag{7}$$

The differential form of the SWEs reads

$$\frac{\partial \mathbf{u}}{\partial t} + \frac{\partial \mathbf{f}}{\partial x} + \frac{\partial \mathbf{g}}{\partial y} = \mathbf{s} \tag{8}$$

or, evaluating the spatial derivatives,

$$\frac{\partial \mathbf{u}}{\partial t} + B\frac{\partial \mathbf{u}}{\partial x} + C\frac{\partial \mathbf{u}}{\partial y} = \mathbf{s}, \tag{9}$$

where

$$B = \frac{\partial \mathbf{f}}{\partial \mathbf{u}}, \qquad C = \frac{\partial \mathbf{g}}{\partial \mathbf{u}} \tag{10}$$

are the Jacobian matrices of the fluxes $\mathbf{f}$ and $\mathbf{g}$ respectively.

Equations (8) are in conservative form, i.e. all the spatial derivatives of the unknowns are in the form of a divergence operator. In the case of a flat bottom ($h_0 = 0$) the right-hand side disappears and we get a strong conservation form. This ensures that a proper discretization of system (1) will automatically capture the weak solutions of the integral form by virtue of the theorem of Lax and Wendroff.[6] It is worthwhile to remember that the SWEs have an infinite hierarchy of conservative forms expressing the conservation of mass, velocity, discharge rate, energy and so on:[7]

$$\frac{\partial}{\partial x} h + \frac{\partial}{\partial x}(hv) = 0,$$

$$\frac{\partial}{\partial x} v + \frac{\partial}{\partial x}\left(\frac{v^2}{2} + h\right) = 0,$$

$$\frac{\partial}{\partial x}(hv) + \frac{\partial}{\partial x}\left(hv^2 + \frac{h^2}{2}\right) = 0,$$

$$\frac{\partial}{\partial x}\left(\frac{v^2 h}{2} + \frac{h^2}{2}\right) + \frac{\partial}{\partial x}\left(\frac{v^3 h}{3} + vh^2\right) = 0,$$

$$\ldots.$$

Any two of these equations are equivalent to one another provided that the solution belongs to C^1. However, when shocks (i.e. bores) are involved, this equivalency does not exist any more, because the Rankine–Hugoniot condition (and not the differential equations any longer) needs

to be satisfied. Consequently, in this latter case the solution depends on the chosen variables. Therefore it is important to stress that the present formulation is based on the requirement that elevation and unit-width discharge are conserved.

The two-dimensional system (9) is hyperbolic; indeed, for any unit vector $\mathbf{n} = (n_x, n_y)^T$ the matrix $A = Bn_x + Cn_y$ is diagonalizable with real eigenvalues and takes the explicit form

$$A = \begin{pmatrix} 0 & n_x & n_y \\ c^2 n_x - v_x \mathbf{v}\cdot\mathbf{n} & v_x n_x + \mathbf{v}\cdot\mathbf{n} & v_x n_y \\ c^2 n_y - v_y \mathbf{v}\cdot\mathbf{n} & v_y n_x & v_y n_y + \mathbf{v}\cdot\mathbf{n} \end{pmatrix}. \tag{11}$$

Here we are making use of the variables celerity c and velocity $\mathbf{v}$ which are related to the conservative ones as follows:

$$c^2 = h, \qquad h\mathbf{v} = \mathbf{q}. \tag{12}$$

The eigenvalues of the matrix A are

$$\lambda^1 = \mathbf{v}\cdot\mathbf{n} - c, \qquad \lambda^2 = \mathbf{v}\cdot\mathbf{n}, \qquad \lambda^3 = \mathbf{v}\cdot\mathbf{n} + c. \tag{13}$$

The right eigenvectors are respectively

$$\mathbf{r}^1 = (1, v_x - cn_x, v_y - cn_y)^T, \qquad \mathbf{r}^2 = (0, n_y, -n_x)^T, \qquad \mathbf{r}^3 = (1, v_x + cn_x, v_y + cn_y)^T, \tag{14}$$

the left eigenvectors are

$$\begin{aligned} \mathbf{l}^1 &= (\tfrac{1}{2} + (\mathbf{v}\cdot\mathbf{n})/2c, -n_x/2c, -n_y/2c)^T, \\ \mathbf{l}^2 &= (v_y n_x - v_x n_y, n_y, -n_x)^T, \\ \mathbf{l}^3 &= (\tfrac{1}{2} - (\mathbf{v}\cdot\mathbf{n})/2c, n_x/2c, n_y/2c)^T \end{aligned} \tag{15}$$

and of course $\mathbf{r}^i \cdot \mathbf{l}^j = \delta_{ij}$.

3. FINITE VOLUME DISCRETIZATION

In this section the finite volume numerical method is introduced. To be more general, the notation used here refers to unstructured grids, although the 2D computation that will be shown in the last section involves a structured grid.

To obtain a finite volume discretization of (1), we start partitioning Ω by a finite union of σ_i (the 'control volumes', which are actually 'control surfaces') with boundary Γ_i. Introducing the cell-averaged variables

$$\mathbf{U}_i = \left(\int_{\sigma_i} \mathbf{u}\, d\sigma \right) \Big/ \Sigma_i, \quad \text{where } \Sigma_i = \int_{\sigma_i} d\sigma, \tag{16}$$

we get the discrete counterpart of the adimensional version of (1):

$$\frac{d}{dt}\mathbf{U}_i + \frac{1}{\Sigma_i} \oint_{\Gamma_i} (\mathbf{f} n_x + \mathbf{g} n_y)\, d\Gamma = 0. \tag{17}$$

A Euler forward explit discretization in time gives

$$\mathbf{U}_i^{n+1} - \mathbf{U}_i^n + \frac{\Delta t}{\sum_i} \oint_{\Gamma_i} \mathbf{z}^n\, d\Gamma = 0, \tag{18}$$

where $\mathbf{z}^n = \mathbf{f}^n n_x + \mathbf{g}^n n_y$ and Δt is the time step.

To discretize in space, we suppose the flux constant along each side of the area Σ_i. Therefore the total flux through Γ_i is the discrete sum of the fluxes through every side of Σ_i:

$$\mathbf{U}_i^{n+1} - \mathbf{U}_i^n + \frac{\Delta t}{\Sigma_i} \sum_k \mathbf{Z}_{ik}^n \, \Delta\Gamma_{ik} = 0, \tag{19}$$

where $\Delta\Gamma_{ik}$ is the length of the segment between the volumes i and k, $\mathbf{Z}_{ik}^n$ represents the discretization of $\mathbf{z}$ on Γ_{ik} at time n and the summation index runs over all the boundary segments of Σ_i.

Finally, the spatial discretization consists of determining how the numerical flux of $\mathbf{Z}_{ik}^n$ depends on the states $\mathbf{U}_i^n$ and $\mathbf{U}_k^n$; we have an upwind scheme if this dependence is not symmetric with respect to each face but shifted in order to favour one of the volumes according to the value of the solution itself.

Precisely, to find the numerical flux between the volumes Σ_i and Σ_k, we consider the numerical solution of the 1D Riemann problem

$$\frac{\partial \mathbf{u}(s,t)}{\partial t} + \frac{\partial \mathbf{z}(\mathbf{u}(s,t))}{\partial s} = 0, \tag{20}$$

where $\mathbf{z} = \mathbf{f}n_x + \mathbf{g}n_y$ and the initial condition is $\mathbf{u} = \mathbf{u}_i$ for $s < 0$ and $\mathbf{u} = \mathbf{u}_k$ for $s > 0$. This hypothesis entails that we restrict ourselves to consider only waves travelling normally to the boundary segment.

We define the numerical flux $\mathbf{Z}(\mathbf{U}_i, \mathbf{U}_k, \mathbf{n})$ as*

$$\mathbf{Z}(\mathbf{U}_i, \mathbf{U}_k, \mathbf{n}) = \mathbf{z}(\mathbf{U}_i) + \sum_{\hat{\lambda}^p < 0} \hat{\mathbf{r}}^p \hat{\lambda}^p [\mathbf{l}^p \cdot (\mathbf{U}_i - \mathbf{U}_k)], \tag{21}$$

where $\hat{\lambda}^p$, $\hat{\mathbf{r}}^p$ and $\hat{\mathbf{l}}^p$ are defined as

$$\hat{\mathbf{r}}^p(\mathbf{U}_i, \mathbf{U}_k, \mathbf{n}) = \mathbf{r}^p(\hat{h}, \hat{\mathbf{v}}, \hat{\mathbf{n}}), \qquad \hat{\mathbf{l}}^p(\mathbf{U}_i, \mathbf{U}_k, \mathbf{n}) = \mathbf{l}^p(\hat{h}, \hat{\mathbf{v}}, \hat{\mathbf{n}}), \qquad \hat{\lambda}^p(\mathbf{U}_i, \mathbf{U}_k, \mathbf{n}) = \lambda^p(\hat{h}, \hat{\mathbf{v}}, \hat{\mathbf{n}}) \tag{22}$$

and $\hat{h}$ and $\hat{\mathbf{v}}$ are the Roe-averaged quantities

$$\hat{h} = \frac{h_i + h_k}{2}, \qquad \hat{v}_x = \frac{\sqrt{h_i} v_{x,i} + \sqrt{h_k} v_{x,k}}{\sqrt{h_i} + \sqrt{h_k}}, \qquad \hat{v}_y = \frac{\sqrt{h_i} v_{y,i} + \sqrt{h_k} v_{y,k}}{\sqrt{h_i} + \sqrt{h_k}}. \tag{23}$$

This definition of $\hat{A}$ ensures that the properties prescribed by Roe for the numerical flux of a conservative law are satisfied[1] and in particular it ensures conservativity:

$$\mathbf{z}(\mathbf{U}_i) - \mathbf{z}(\mathbf{U}_k) = \hat{A}(\mathbf{U}_i - \mathbf{U}_k). \tag{24}$$

Finally, the first-order numerical discretization we use to approximate problem (1) is

$$\mathbf{U}_i^{n+1} - \mathbf{U}_i^n + \frac{\Delta t}{\Sigma_t} \sum_k \mathbf{Z}(\mathbf{U}_i, \mathbf{U}_k, \mathbf{n}) \Delta\Gamma_{ik} = 0, \tag{25}$$

where $\mathbf{Z}$ is as defined in (21).

It can be easily shown that for a linear hyperbolic system of equations the above method based on the solution of the Riemann problem will reproduce a first-order one-sided scheme. It is rather intuitive that an improvement in (25) can be achieved by supposing a linear (rather than constant) solution in every volume. It can be shown that such a modification yields an

* For notational simplicity we omit the time index from now on without any possibility of confusion, because the flux always depends on the solution at time t^n.

algorithm which is analogous to the celebrated Lax–Wendroff scheme.[4,6] On the other hand, it is also well known that on a Cartesian mesh such a second-order finite difference scheme, although very accurate in the smooth solution regions, causes unphysical oscillations near the discontinuities. To obviate this undesired effect, it is necessary to modify in a suitable way the slopes in every volume. This goal can be achieved by the introduction of a 'flux limiter', an extensive review of which can be found in Reference 8. The generic flux **Z** obtained by this procedure can be written as

$$\mathbf{Z} = \mathbf{Z}_{\text{low}} + \phi(\mathbf{Z}_{\text{high}} - \mathbf{Z}_{\text{low}}), \tag{26}$$

where the flux limiter ϕ depends on the local solution gradient as follows: it is about zero near the discontinuities and about unity in the smooth flow regions. These ideas were originally introduced by van Leer with his MUSCL scheme.[9]

In the following test cases we have used the van Leer flux limiter, which for the sake of simplicity we write here for the case of a linear scalar equation $u_t + au_x = 0$ with $a > 0$:

$$\phi(\theta_j) = \frac{|\theta_j| + \theta_j}{1 + |\theta_j|}, \quad \text{where } \theta_j = \frac{U_{j+1} - U_j}{U_j - U_{j-1}}. \tag{27}$$

Finally, considering the definition in (21) as the low-order flux, the slope-limiting correction we use in the present context is

$$Z^q(\mathbf{U}, ik) = Z^q_{\text{low}}(\mathbf{U}, ik) + \frac{1}{2}\sum_{p=1}^{3} \hat{\lambda}^p_{ik}\left(\text{sgn}(\hat{\lambda}^p_{ik}) - \frac{\Delta t}{\Delta s_{ik}}\hat{\lambda}^p_{ik}\right)\Delta s_{ik}\hat{\gamma}^p_{ik}\hat{r}^{qp}_k\phi(\hat{\gamma}^p_{ik}\hat{r}^{qp}_k, \hat{\gamma}^p_{i1}\hat{r}^{qp}_{i1}), \tag{28}$$

where Δs_{ik} is the distance between the centroids of the ith and kth volumes, the index q indicates the qth component of a vector,

$$\gamma^p_{ik} = \mathbf{l}^p \cdot (\mathbf{U}_i - \mathbf{U}_k) \tag{29}$$

and the index $i1$ indicates another volume side suitably chosen. In the case of structured meshes the $i1$th side will be the backward or the forward one depending on the sign of $\hat{\lambda}^p_{ik}$. In smooth flow regions $\phi \simeq 1$ and the Lax–Wendroff scheme for the characteristic variables may be recovered. The details of this scheme may be found for the Euler framework in References 4 and 8. It is very attractive because it preserves the Lax–Wendroff scheme advantages when the solution is smooth and, in particular, second-order accuracy in time is achieved in one integration step.

The wall boundary conditions are implemented in a standard way defining a dummy reflection cell out of the boundary with the same value of the solution as in the boundary cell, except for the normal velocity which has the same magnitude but opposite sign. The Riemann problem with these initial conditions gives a solution $\mathbf{u}$ with zero normal velocity on the boundary, which is exactly what defines the solution therein.

4. DAM BREAK WAVE ON DRY BOTTOM

In this section we recall the exact solution of the classical dam greak problem using hyperbolic systems theory. This derivation will be helpful in discussing the numerical resutls in the last

section. Consider the 1D SWE differential system

$$\frac{\partial}{\partial t} h + \frac{\partial}{\partial x} q = 0, \qquad \frac{\partial}{\partial t} q + \frac{\partial}{\partial x}\left(\frac{q^2}{h} + \frac{h^2}{2}\right) = 0, \tag{30}$$

to be solved with the initial conditions

$$\mathbf{u} = \begin{cases} \mathbf{u}_L = (H, 0) & \text{if } x < 0, \\ \mathbf{u}_R = (0, 0) & \text{if } x > 0. \end{cases}$$

This problem can be solved by simple wave theory:[7] the left and right states can be connected by just one wave of rarefaction type. In fact, in the 1D framework we have just two eigenvalues, $\lambda^1 = v - \sqrt{h}$ and $\lambda^2 = v + \sqrt{h}$. We look for a similarity solution $\mathbf{u}(x/t)$ such that for $x/t = \lambda^1$ is it equal to the left state,

$$\mathbf{u}(-\sqrt{H}) = \mathbf{u}_L, \tag{31}$$

i.e. $h(-\sqrt{H}) = H$ and $q(-\sqrt{H}) = 0$. Under this assumption the partial differential system (30) becomes a system of ordinary differential equations

$$-(x/t)h' + hv' + vh' = 0, \qquad -(x/t)v' + vv' + h' = 0, \tag{32}$$

where the prime denotes the derivative with respect to x/t. Here we can equivalently use the primitive variables h and v, because the solution is assumed to be smooth. The integration of (32) together with boundary conditions (31) gives the solution

$$h(x/t) = \tfrac{1}{9}(2\sqrt{H} - x/t)^2, \qquad v(x/t) = \tfrac{2}{3}(x/t + \sqrt{H}) \tag{33}$$

and its domain of definition is bounded by $-\sqrt{H} < x/t$. Moreover, we note that the value of the conservative variables (h, q) given by (33) coincides with the right state for $x/t = 2\sqrt{H}$; therefore this wave can be extended to the right until the state $\mathbf{u}_R$ is reached and the global solution is finally given by (33) defined in $-\sqrt{H} < x/t < 2\sqrt{H}$.

It should be remarked that this solution is only valid using the unknowns (h, q). If the primitive variables are used, the use of the Rankine–Hugoniot condition leads to a very different weak solution composed of two jumps.

5. STILL WATER ON UNEVEN BOTTOM

The numerical method proposed in Section 3 provides accurate results on test problems with a flat bottom, as will be shown in the next section for several test cases. At a first look such effectiveness seems to be lost when the bottom slope varies. Let us consider again the 1D SWEs with initial conditions

$$h(x, 0) = h_0(x), \qquad q(x, 0) = 0, \tag{34}$$

where $h_0(x)$ is a non-constant function. It is trivial to check that the exact solution coincides with the initial conditions at any time (i.e. nothing moves). Unfortunately, this feature is not ensured by our discrete solution. In fact, suppose that we want to update the $\mathbf{U}_j$-value using the 1D counterpart of the first-order scheme (25). At the first time step we would have

$$\mathbf{U}_j^1 = \mathbf{U}_j^0 - \frac{\Delta t}{\Delta x}\left[\mathbf{F}(\mathbf{U}_j, \mathbf{U}_{j+1}) - \mathbf{F}(\mathbf{U}_{j-1}, \mathbf{U}_j)\right] + \Delta t \mathbf{S}_j, \tag{35}$$

where $\mathbf{S}_j$ is a discretization of the source term s in the jth interval and

$$\mathbf{F}(\mathbf{U}_j, \mathbf{U}_{j+1}) = \mathbf{f}(\mathbf{U}_j) + \sum_{\hat{\lambda}^p < 0} \hat{\mathbf{r}}^p \hat{\lambda}^p [\mathbf{l}^p \cdot (\mathbf{U}_{j+1} - \mathbf{U}_j)], \tag{36}$$

$$\mathbf{F}(\mathbf{U}_{j-1}, \mathbf{U}_j) = \mathbf{f}(\mathbf{U}_{j-1}) + \sum_{\hat{\lambda}^p < 0} \hat{\mathbf{r}}^p \hat{\lambda}^p [\mathbf{l}^p \cdot (\mathbf{U}_j - \mathbf{U}_{j-1})]. \tag{37}$$

In this 1D case the eigenvalues and eigenvectors are

$$\lambda^1 = v - c, \qquad \lambda^2 = v + c, \tag{38}$$

$$\mathbf{r}^1 = (1, v - c)^{\mathrm{T}}, \qquad \mathbf{r}^2 = (1, v + c)^{\mathrm{T}}, \tag{39}$$

$$\mathbf{l}^1 = ((1 + v/c)/2, -1/2c)^{\mathrm{T}}, \qquad \mathbf{l}^2 = ((1 - v/c)/2, 1/2c)^{\mathrm{T}}. \tag{40}$$

By some calculations it may then be found that

$$\mathbf{F}(\mathbf{U}_j, \mathbf{U}_{j+1}) = (-\tfrac{1}{2}\hat{c}_{j+1/2}(h_{j+1} - h_j), \tfrac{1}{2}h_j^2 + \tfrac{1}{2}\hat{c}_{j+1/2}^2(h_{j+1} - h_j))^{\mathrm{T}}, \tag{41}$$

where $\hat{c}_{j+1/2} = \sqrt{[(h_{j+1} + h_j)/2]}$. As may be easily seen, for any discretization of the source term the updated value of h is different from h_0, which is fairly undesirable. However, the error for the computed solution is first-order. In fact, let us suppose that we discretize the source term as

$$\mathbf{S}_j = \left(0, \frac{1}{4\Delta x}(h_{j+1}^2 - h_{j-1}^2)\right)^{\mathrm{T}}. \tag{42}$$

Performing a Taylor series expansion of the unknowns around $x = x_j$, we find the error after a single time step, defined as the difference between the exact and the computed solution:

$$\begin{aligned}
\mathbf{U}^{1,\mathrm{exact}}(x_j) - \mathbf{U}_j^1 &= \frac{\Delta t}{\Delta x}[\mathbf{F}(\mathbf{U}_j, \mathbf{U}_{j+1}) - \mathbf{F}(\mathbf{U}_{j-1}, \mathbf{U}_j)] + \Delta t \mathbf{S}_j \\
&= \frac{\Delta t}{\Delta x}\left(-\frac{1}{2\sqrt{2}}\sqrt{(h_{j+1} + h_j)}(h_{j+1} - h_j) + \frac{1}{2\sqrt{2}}\sqrt{(h_j + h_{j-1})}(h_j - h_{j-1}), 0\right)^{\mathrm{T}} \\
&= \Delta t\left(\frac{1}{4\sqrt{(2h_j)}}\alpha^2 \Delta x + O(\Delta x^2), 0\right)^{\mathrm{T}},
\end{aligned} \tag{43}$$

where

$$\alpha = \left.\frac{\mathrm{d}h_0}{\mathrm{d}x}\right|_{x = x_j}. \tag{44}$$

Therefore, although it might be very disappointing that the constant still water solution is not exactly computed, it is worthwhile to remember that the formal order of accuracy of the scheme is achieved. Moreover, the form of the error that appears in (43) shows that the loss of accuracy becomes more severe as h gets nearer to lower values, i.e. on approaching the coast.

The reason for this behaviour is that in a Godunov-type approach the solution is computed as a flux balancing of waves that do not really exist. Riemann solver schemes rely on the assumption of straight characteristic slopes, which is no longer satisfied when source terms appear. A discussion about this intrinsic limitation of Riemann solvers is given in Reference 10 and an *ad hoc* remedy in a specific case is described in Reference 11. However, when the exact solution is not constant, the present splitting approach shows other attractive features over schemes that compute the above solution exactly, as could be the case of the classic McCormack scheme.[12]

6. NUMERICAL RESULTS

6.1. *Dam break on dry bottom*

Here we consider the numerical approximation of the problem described in Section 4 with the aim of comparing numerical and exact solutions. This SWE test case has the peculiar feature that for $x/t \to 2\sqrt{H}$ the elevation goes to zero while the velocity retains a finite value. Therefore the two eigenvalues collapse into $\lambda = v$, the Froude number $Fr = v/c$ goes to infinity and the system is not strictly hyperbolic any more. At $x/t = 2\sqrt{H}$ the governing equation is therefore $dv/dt = 0$ and the entire system can be restated as a free boundary problem.[13,14]

The initial conditions we have used are

$$\mathbf{u}_L = (10, 0), \qquad \mathbf{u}_R = (0, 0). \tag{45}$$

We consider a domain of length 100 divided into 150 equally spaced intervals. We perform 70 interations in time using a time step $\Delta t = 0{\cdot}1$. The results are shown in Figure 2.

The discretization is monotonic and accurate everywhere. The computations are performed using the van Leer limiter, except near the smallest $h(h < 10^{-2})$ where a first-order approximation is used to avoid negative elevation at all. The error is negligible except in a small neighbourhood of $x/t = 2\sqrt{H}$ were strict hyperbolicity fails; anyway, the error is relevant only for the velocity, which is discontinuous therein.

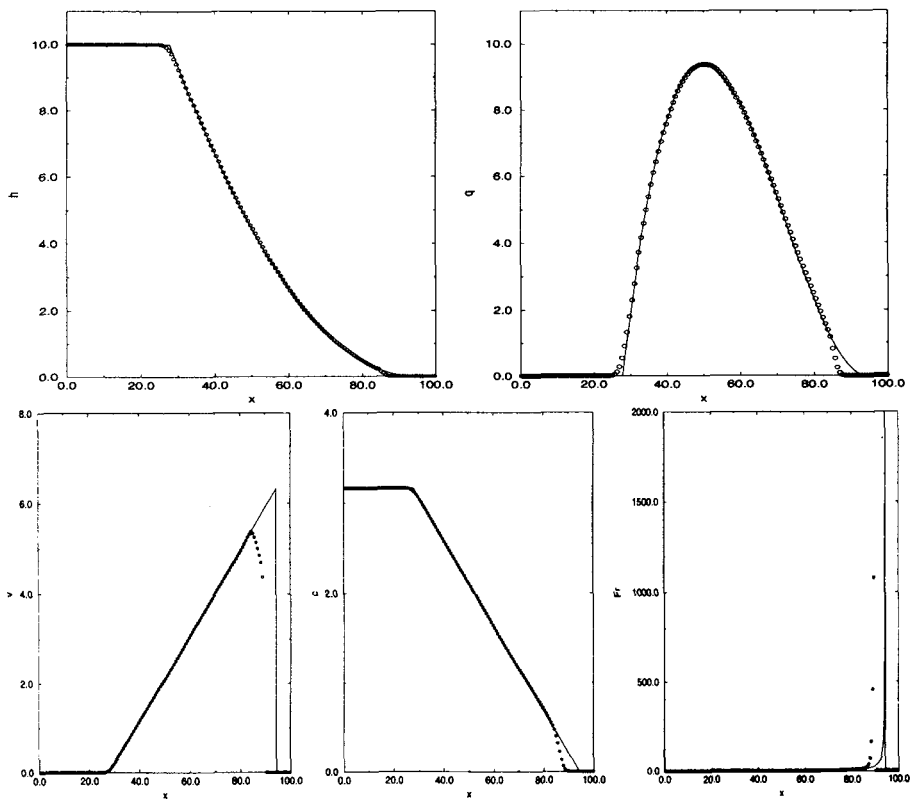

Figure 2. Dam break on dry bottom: comparison between numerical results (circles) and analytical solution (line)

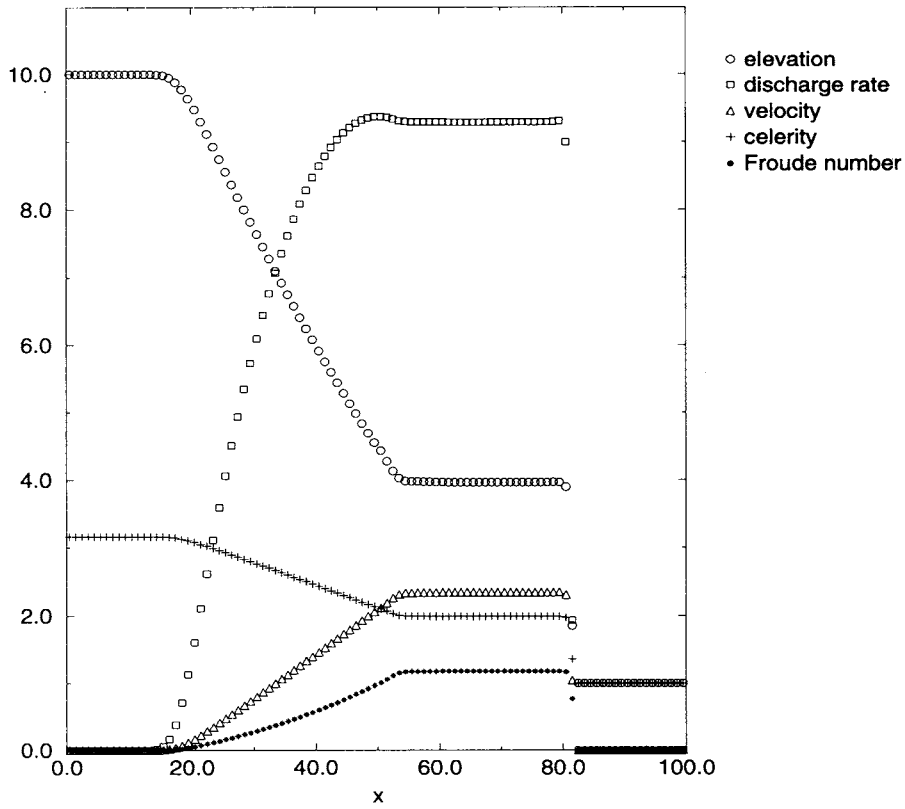

Figure 3. Dam break on wet bottom

6.2. *1D dam break in a basin*

This second test is found more often in the literature: analogous computations for comparison can be found in References 2 and 3. The initial states we consider are

$$\mathbf{u}_L = (10, 0), \qquad \mathbf{u}_R = (1, 0). \tag{46}$$

Note that the non-zero elevation of the right state avoids flooding and all associated difficulties. The computational domain length is 100, 100 spatial nodes are used, the time step is 0·2 and 60 iterations in time are performed.

In Figure 3 the elevation h, velocity v, discharge q, celerity c and Froude number Fr versus x are plotted. The bore wave is captured in one cell and oscillations are absent. The results are very similar to those presented in Reference 3; in both cases the bore wave is captured in one cell, although in Reference 3 the more compressive superbee flux limiter is used.

6.3. *2D dam break in a reservoir*

The basin geometry and dimensional parameters used in this computation are the same as suggested in Reference 15 and may be seen in Figure 4.

The initial states are

$$\mathbf{u}_L = (10\ \text{m}, 0\ \text{m}^2\ \text{s}^{-1}, 0\ \text{m}^2\ \text{s}^{-1}), \qquad \mathbf{u}_R = (5\ \text{m}, 0\ \text{m}^2\ \text{s}^{-1}, 0\ \text{m}^2\ \text{s}^{-1}). \tag{47}$$

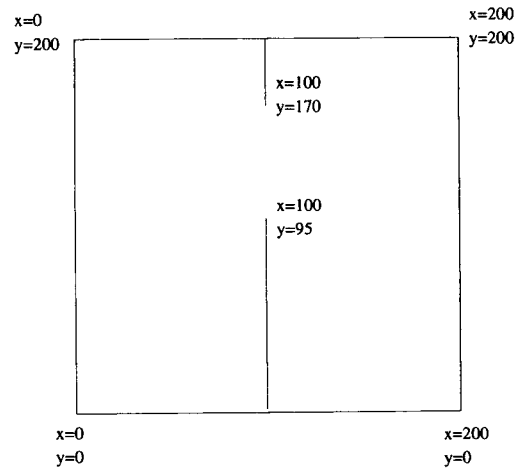

Figure 4. Reservoir geometry for partial dam failure test

A uniform Cartesian grid of 40 × 40 volumes is used and 20 iterations in time are performed until the final time of 7·2 s. A comparison with the results presented in References 2 and 3 is not easy, because isosurfaces are less easy to read than 1D graphics. However, the solutions look very similar. The only difference is that the wave rising up the left wall in Reference 3 seems to be higher than the level in the rest of the box, while in Reference 2 the present work (Figure 5) it looks lower.

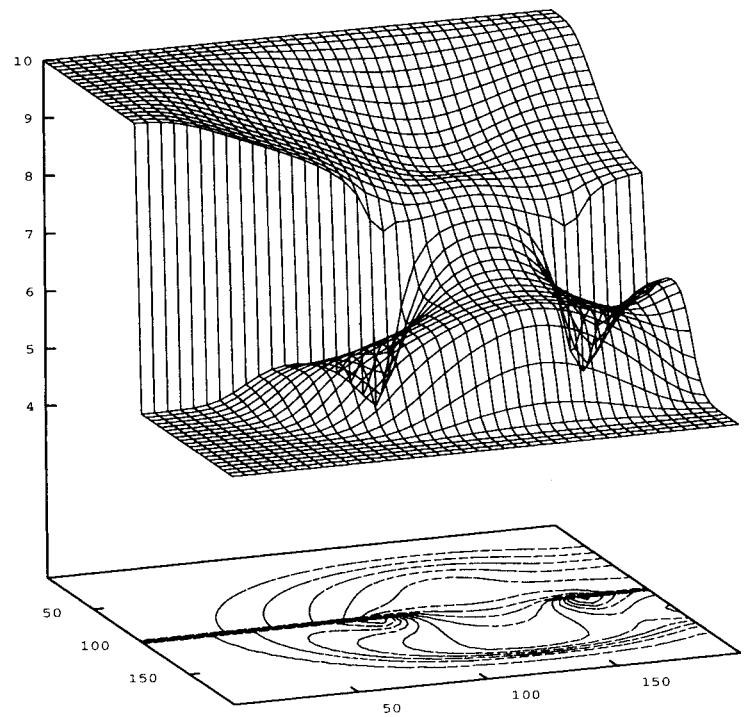

Figure 5. Partial dam break in reservoir

7. CONCLUSIONS

Roe's approximate Riemann solver enhanced by slope limiting has been applied to the shallow water equations. Some peculiar features that arise in this context are focused on and discussed. The analysis carried out and the numerical results presented suggest the following remarks.

1. It has been pointed out previously that mathematical difficulties can arise in the dry–wet region. However, using the present approach, no front tracking is necessary for the dry–wet boundary, the solution retains monotonicity everywhere and the inaccuracy found in this region does not affect the global solution quality.
2. The present scheme combines second-order accuracy in time if the solution is smooth with the capability to compute discontinuities sharply and monotonically as standard first-order schemes do.
3. We have focused on the difficulties that arise when dealing with varying bottom terms by the flux difference approach, giving a quantitative evaluation of the error of the scheme.

ACKNOWLEDGEMENT

The author is indebted to Luigi Quartapelle for many fruitful discussions. This research has been carried out with the support of the Sardinia Regional Authorities.

REFERENCES

1. P. L. Roe, 'Approximate Riemann solvers, parameter vectors and difference schemes', *J. Comput. Phys.*, **43**, 357–372 (1981).
2. F. Alcrudo and P. Garcia-Navarro, 'A high resolution Godunov type scheme in finite volumes for the 2D shallow water equations', *Int. j. numer. methods fluids*, **16**, 489–505 (1993).
3. P. Glaister, 'Flux difference splitting for open channel flow', *Int. j. numer. methods fluids*, **16**, 629–654 (1993).
4. R. J. LeVeque, *ETH Zurich Lectures in Mathematics, Numerical Methods for Conservation Laws*, Birkhäuser, 1990.
5. V. I. Agoshkov, D. Ambrosi, V. Pennati, A. Quarteroni and F. Saleri, 'Mathematical and numerical modelling of shallow water flow', *Comput. Mech.*, **11**, 280–299 (1993).
6. P. D. Lax and B. Wendroff, 'Systems of conservation laws', *Commun. Pure Appl. Math.*, **13**, 217–237 (1960).
7. G. B. Whitham, *Linear and Non Linear Waves*, Wiley, New York, 1974.
8. P. K. Sweby, 'High resolution schemes using flux limiters for hyperbolic conservation laws', *SIAM J. Numer. Anal.*, **21**, 995–1011 (1984).
9. B. van Leer, 'Towards the ultimate conservative difference scheme V—a second order sequel to Godunov's method', *J. Comput. Phys.*, **32**, 101–136 (1979).
10. P. K. Sweby, in *Notes on Numerical Fluid Mechanics*, Vol. 24, Vieweg, Braunschweig, 1989, p. 599.
11. G. Watson, D. H. Peregrine and E. F. Toro, 'Numerical solution of the shallow water equations on a beach using the weighted average flux method', *Computational Fluid Dynamics '92*, Elsevier, Amsterdam, 1992.
12. C. V. Bellos, J. V. Soulis and J. G. Sakkas, 'Computation of dam-break induced flow', *Adv. Water Resources*, **14**, 31–41 (1991).
13. R. Fazio and D. J. Evans, 'An implicit difference scheme for a moving boundary hyperbolic problem', *Appl. Numer. Math.*, **12**, 485–496 (1993).
14. R. E. Grundy and J. W. Rottman, 'The approach to self similarity of the solutions of the shallow-water equations representing gravity-current releases', *J. Fluid Mech.*, **156**, 39–53 (1985).
15. R. J. Fennema and M. H. Chaudry, 'Explicit methods for 2D transient free-surface flows', *J. Hydraul. Eng. ASCE*, **116**, 1013–1034 (1990).
16. D. Ambrosi 'Un metodo numerico per correnti comprimibili non stazionarie', *Tesi di Dottorato*, Milano, 1993.
17. S. K. Godunov, 'A difference scheme for numerical computation of discontinuous solutions of equations of fluid dynamics', *Math. Sb.*, **47**, 271–306 (1959); *US JPRS Transl. 7226*, 1960.
18. A. Harten, 'High resolution schemes for hyperbolic conservation laws', *J. Comput. Phys.*, **49**, 357–393 (1983).
19. A. Harten and J. M. Hyman, 'Self adjusting grid methods for one dimensional hyperbolic conservation laws', *J. Comput. Phys.*, **50**, 235–269 (1983).
20. A. Harten, P. D. Lax and B. van Leer, 'On upstream differencing and Godunov-type schemes for hyperbolic conservation laws', *ICASE Rep. 82-5*, 1982 *SIAM Rev.*, (1983).
21. P. D. Lax, *Hyperbolic Systems of Conservation Laws and the mathematical Theory of Shock Waves*, SIAM, Philadelphia, PA, 19XX.
22. H. Nessayahu and E. Tadmor, 'Non-oscillatory central differencing for hyperbolic conservation laws', *J. Comput. Phys.*, **87**, 408–463 (1990).